Photoisomerization of *cis,cis*- to *trans,trans*-1,4-Diaryl-1,3-butadienes in the Solid State: The Bicycle-Pedal Mechanism

Jack Saltiel,* Tallapragada S. R. Krishna, Somchoke Laohhasurayotin, Katy Fort, and Ronald J. Clark

Department of Chemistry and Biochemistry, Florida State University, Tallahassee, Florida 32306-4390

Received: September 12, 2007; In Final Form: October 12, 2007

The photoisomerizations of crystalline or powdered *cis,cis*-1,4-diphenyl- and 1,4-di(*o*-tolyl)-1,3-butadienes (*cc*-DPB and *cc*-DTB) to the trans,trans isomers were studied at room temperature. The progress of the reactions was monitored by fluorescence spectroscopy, powder X-ray diffraction, ^{1}H NMR, and high-performance liquid chromatography. Conversions to the trans,trans isomers were as high as 90% for *cc*-DPB and 20% for *cc*-DTB. Formation of the cis,trans isomers, the sole products obtained in solution and in very viscous glassy media at 77 K, is completely suppressed in the solid state. The observed two-bond photoisomerizations are explained by the bicycle-pedal (BP) photoisomerization mechanism. X-ray structure determinations show that *o*-methyl substitution causes a widening of the phenyl/diene dihedral angles from 40° to 56° and decreases the number of conformers in the crystal from two in *cc*-DPB to one in *cc*-DTB. The two conformers of *cc*-DPB molecules exist in crystals in edge-to-face alternating arrays, one of which has the two phenyls in parallel planes and the other in roughly perpendicular planes. The edge-to-face relationship is maintained in *cc*-DTB, but only the conformer with the *o*-tolyl groups in parallel planes is present. The time evolutions of fluorescence spectra measured in the course of the photoreaction show remarkable similarities, despite the different molecular conformations and crystal packing arrangements. Principal component analyses of the spectral matrices indicate the formation of discrete components, suggesting that the two-bond photoisomerizations proceed in stages involving molecules in different microcrystal environments. The structureless appearances of the initial fluorescence spectra show that the reactions are in part diabatic. The BP mechanism can account for the observations if the bicycle-pedal motion began in the excited state, S_1, and were completed in the ground state, S_0. Analysis of void spaces in the crystal lattice reveals much less compact packing of *cc*-DPB than of *cc*-DTB molecules, possibly explaining the much higher conversions to photoproduct from *cc*-DPB.

Introduction

Observations by Zechmeister[2] and co-workers showing that following direct excitation in solution the photoisomerization of the 1,4-diphenyl-1,3-butadienes (DPBs)[1] proceeds sequentially one bond at a time were confirmed by Whitten[3] and Yee[4] and their co-workers who further concluded that it was a singlet excited-state reaction. Whitten and co-workers proposed that it occurs via torsional relaxation (one-bond twist, OBT) to non-interconverting phenallylbenzyl intermediates[3] analogous to the twisted intermediates proposed by Saltiel and co-workers for

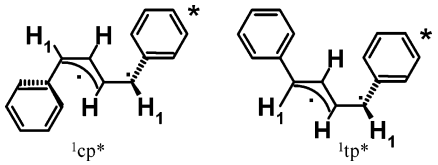

^{1}cp* ^{1}tp*

the stilbenes[5] and the 2,4-hexadienes.[6] Whereas both intermediates can be accessed from the S_1 state of the cis,trans isomer (*ct*-DPB), *tt*-DPB and *cc*-DPB give only intermediates with *trans*-phenallyl (^{1}tp*) and *cis*-phenallyl (^{1}cp*) groups, respectively.

Solvent friction inhibits torsional relaxation in olefins as reflected in diminished photoisomerization quantum yields and enhanced fluorescence quantum yields.[1,7] Extensive research, especially by Fischer[8] and Alfimov[9] and their co-workers, has shown that activated photoisomerization of trans isomers is entirely suppressed at 77 K in glassy media, whereas the photoisomerization of cis isomers often persists, albeit much less efficiently than in solution. Two alternative mechanisms involving concerted rotation about more than one bond in S_1, initially postulated to explain the specificity and high photoisomerization quantum yields of the retinyl moieties of rhodopsin and bacteriorhodopsin, have been considered recently in accounting for photoisomerization in volume-confining media, generally: the bicycle-pedal mechanism (BP), which involves simultaneous rotations in S_1 about two C−C double bonds of a polyene,[10] and the Hula-twist mechanism (HT), which involves simultaneous rotation about a double bond and an adjacent essential single bond (equivalent to a 180° translocation of one CH unit).[11] Those two mechanisms are assumed to reduce volume requirements associated with torsional relaxation by confining most of the motion to the vicinity of the isomerizing double bonds, while minimizing the motion of bulky substituents. The claim that tachysterol products obtained on irradiation of previtamin D at 92 K in ether/isopentane/ethyl alcohol (EPA; 5:5:2) glass are those predicted by the HT process[12] stimulated

* Author to whom correspondence should be addressed. E-mail: saltiel@chem.fsu.edu.

10.1021/jp077342c CCC: $40.75
Published on Web 12/22/2007

SCHEME 1: OBT, HT, and BP Mechanisms Applied to *cc*-DPB

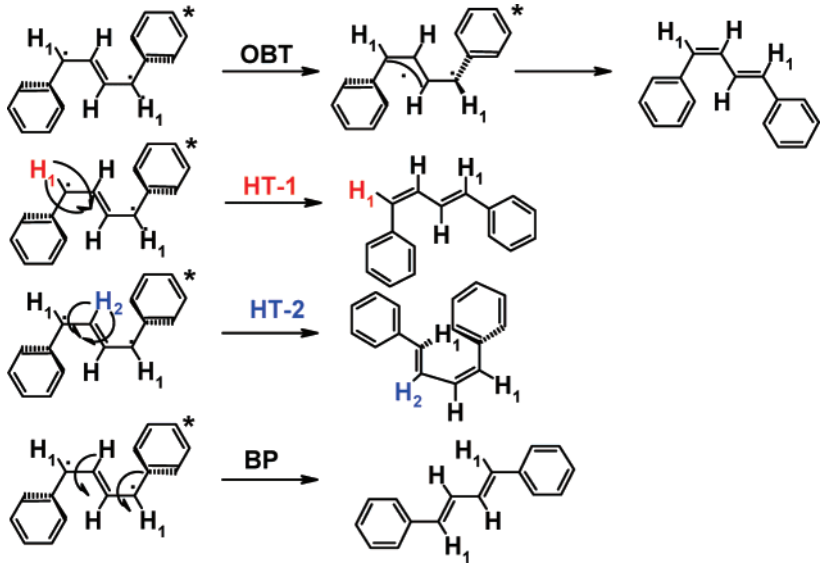

SCHEME 2: OBT and HT-1 Mechanisms Applied to *ct*-DTB

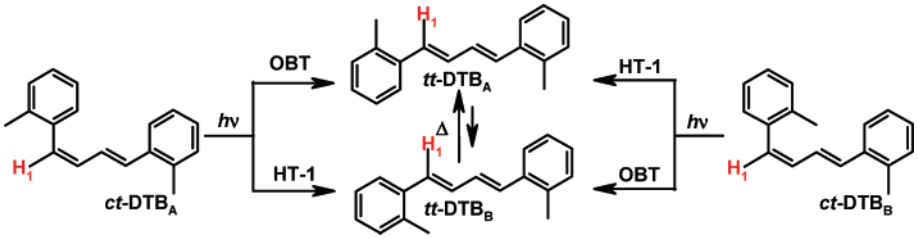

the revival of the HT mechanism[13] and led to the re-examination of the photoisomerization of the DPBs in organic glasses at 77 K[14,15] and in the solid state.[17] Irradiation of *cc*-DPB in glassy media of relatively high viscosity, EPA[14] or methylcyclohexane[15] at 77 K,[16] gives only *ct*-DPB, the one-bond photoisomerization product, as in solution. Spectroscopic observations show that in the rigid glasses the *ct*-DPB product forms as the s-trans conformer, consistent with OBT in fluid solution.[2−4] However, *ct*-DPB formation was attributed to the HT process (HT-1) about the benzylic CH of the diene moiety.[14] When *cc*-DPB is irradiated in the soft isopentane glass[15] at 77 K, formation of *ct*-DPB is accompanied by formation of *tt*-DPB as a major primary photoproduct, consistent with competitive isomerization by the BP mechanism. The different photoisomerization mechanisms are illustrated for *cc*-DPB in Scheme 1. The expected reversal of double/single bond character in the diene moiety of DPB on excitation to S_1 is emphasized in Scheme 1, but other important structural changes, such as increased double bond character in the phenyl−vinyl bonds, are also expected.

Because HT-1 and OBT photoisomerization products from the cis DPB isomers are indistinguishable, the photoisomerization of *cis,trans*-1,4-di-*o*-tolyl-1,3-butadiene (*ct*-DTB) in EPA at 77 K was studied, with the expectation that starting from the assumed more stable conformer, *ct*-DTB$_A$, HT-1 and OBT mechanisms would give unstable (*tt*-DTB$_B$) and stable (*tt*-DTB$_A$) conformers, respectively (Scheme 2).[14] Claims to the contrary notwithstanding,[14] that study too failed to distinguish between OBT and HT-1 mechanisms. As shown in Scheme 2, both mechanisms will account for the formation of a nonequilibrium mixture of *tt*-DTB$_A$ and *tt*-DTB$_B$ conformers.[15]

Our observation of *cc*-DPB → *tt*-DPB two-bond photoisomerization in isopentane glass, the first experimental demonstration of the BP process at low temperature, encouraged us to investigate the photoisomerizations of *cc*-DPB and *cc*-DTB in the solid state at room temperature. We published a preliminary report showing that the irradiation of *cc*-DPB crystals or powder gives isomerization to *tt*-DPB exclusively, consistent with the BP mechanism.[17] A recent review, which failed to cite our *cc*-DPB paper, reported two-bond cis,cis to trans,trans photoisomerization on irradiation of *p,p′*-difluoro- and *p,p′*-dimethoxy-*cc*-DPB crystals.[18] In this paper, we present a more detailed account of our *cc*-DPB work together with analogous observations on the solid-state photoisomerization of *cc*-DTB.

Experimental Section

Materials. *tt*-DPB (Aldrich, reagent) and *cc*-DPB crystals were obtained from ethanol[2a] and methanol,[2b] respectively, as previously described. 1,4-Di(*o*-tolyl)-1,3-butadiyne, obtained via Eglinton reaction coupling of *o*-tolylacetylene (Aldrich) in the presence of copper(I) iodide and oxygen,[19] was reduced to *cc*-DTB by hydrogenation over Lindlar Pd. *ct*-DTB and *tt*-DTB were obtained from *cc*-DTB by 313 nm irradiation in N_2-saturated hexane and refluxing in benzene in the presence of I_2, respectively, as previously described for DPB.[2] The DTB isomers were purified by chromatography on alumina (hexane eluent) and recrystallization from methanol (*cc*- and *ct*-DTB) and ethanol (*tt*-DTB) and characterized by ^{1}H NMR spectroscopy. Our ^{1}H NMR spectra (300 MHz, $CDCl_3$) for the DTB isomers differ somewhat from those reported recently.[14] They are as follows: *cc*-DTB δ 7.39−7.34 (m, 2H), 7.23−7.18 (m, 6H), 6.57 (s, 4H), 2.29 (s, 6H); *ct*-DTB δ 7.42−7.31 (m, 2H), 7.22−7.18 (m, 3H), 7.14−7.10 (m, 3H), 7.07−6.89 (m, 2H), 6.59−6.47 (m, 2H), 2.38 (s, 3H), 2.31 (s, 3H); *tt*-DTB δ 7.57 (d, J = 7.2 Hz, 2H), 7.24−7.16 (m, 6H), 6.912 and 6.908 (dd, prominent peaks of AB pattern, 4H), 2.40 (s, 6H).

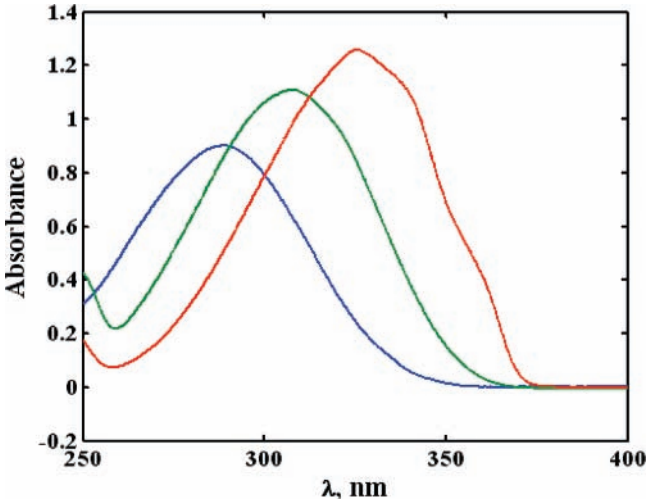

Figure 1. Absorption spectra of *cc*- (blue), *ct*- (green), and *tt*-DTB (red) in cyclohexane at 25 °C.

Irradiation Procedures. Solid crystal or powdered samples (4−20 mg), placed between two glass slides (Fisher brand microscope glass plates) and secured with rubber bands, were irradiated at ambient temperature at 313 nm (potassium perchromate/potassium carbonate filter solution 1.52 and 31.2 g/L, respectively, 7−54 Corning glass filter) or at 366 nm (Corning glass filters 0-52 and 7-37) using 200 or 450 W Hanovia medium-pressure Hg lamps (Ace Glass). Alternatively, the samples were irradiated directly in the sample compartment of a Hitachi F-4500 fluorimeter (2.5 nm slits, 150 W Xe lamp) or externally using a 150 W Xe lamp and a Bausch and Lomb high-intensity monochromator. For powder X-ray diffraction measurements, samples were placed on a single glass slide.

Analytical Procedures. Reaction progress was monitored by fluorescence spectroscopy (Hitachi F-4500 fluorimeter, 2400 nm/min, excitation and emission slits 1.0/2.5 nm, and PMT 700 V), ^{1}H NMR (300 MHz Varian model Gemini 2000 or 270 MHz IBM/Bruker spectrometers; $CDCl_3$), and high-performance liquid chromatography (HPLC; Beckman Coulter gold system with 125 and 166 solvent and detector modules, respectively; a Beckman Ultra sphere 0.5 μm silica 4.6 × 250 mm^2 column was employed with *n*-hexane mobile phase, 0.5 mL/min flow rate, and detector λ set at 315 nm; correction factors were based on DPB isomer spectra in *n*-hexane, which agreed with those given in ref 2). Spectra for the DTB isomers in cyclohexane are shown in Figure 1 (λ_{max} = 288.4, 308.4, and 325.6 nm; $\epsilon_{max} = 2.02 \times 10^4$; 2.61×10^4, and 3.09×10^4 cm^{-1} M^{-1}, for *cc*-, *ct*-, and *tt*-DTB, respectively). For irradiations in the fluorimeter, only a small portion was exposed to light, and it was important not to change the position of the glass slides when monitoring the progress of the reaction by fluorescence spectroscopy.

X-ray Diffraction. Powder X-ray diffraction patterns were measured before and after 366 nm irradiation of mortar and pestle powdered *cc*-DPB samples (~5 mg). The X-ray diffraction data were collected with the use of a Rigaku X-ray diffractometer Ultima III (scan angle 7−31°, 176 kW, 0.01° resolution, 1.5418 Å, slits 0.5 nm, 600 s for data collection, and calibrated to silicon). Fluorescence spectra and ^{1}H NMR spectra of the powdered samples were recorded following the powder X-ray diffraction measurements for different irradiation intervals. Crystallographic data for *cc*-DTB: $C_{18}H_{18}$, M = 234.32, monoclinic, space group $P2(1)/n$, a = 7.6674(7) Å, b = 11.6572(11) Å, c = 7.6942(7) Å, 90°, 92.136°, 90°, V = 673.49(11) Å^3, α = 90°, β = 101.674(2)°, γ = 90°, ρ_{calcd} = 1.155 Mg/m^3, and Z = 2. A Bruker SMART APEX diffractometer at a detector distance of 5 cm with the sample at 173(2) K and Mo Kα radiation (λ = 0.71073 Å) was used to take 2400 frames with a 20 s collection time. The result was 7883 reflections with 1385 ($I > \sigma(I)$, R(int) = 0.0207) being independent and a data to parameter ratio of more than 10:1. Integration was performed using the SAINT program, which is part of the Bruker suite of programs. Absorption corrections made using SADABS, XPREP showed the space group to be $P2(1)/n$, and the structure was solved by direct methods and refined by SHELXTL. The non-hydrogen atoms were refined anisotropically, and the hydrogens were found by least-squares refinement. The R_1 indices ($I > 2\sigma(I)$) based upon all data were R_1 = 0.0531 and wR_2 = 0.1147, and the largest difference peak and hole were 0.263 and −0.199 e Å^{-3}, respectively; goodness of fit on F^2 is 1.217. For the data analysis and crystallographic data in CIF electronic format, see the Supporting Information.

Figure 2. X-ray structure of *cc*-DPB. The four molecules in the asymmetric unit are viewed roughly end on.[15]

Data Analysis. Pretreatment of the fluorescence spectra (baseline corrections) and principal component analysis (PCA) calculations[20] were performed on a Dell microcomputer working with appropriate routines in the environment of MATLAB packages, versions 5.2 and 6.1.

Computational Details. Calculations were performed with the Gaussian 98 program package[21] with gradient geometry optimization.[22] All geometries were fully optimized using the B3LYP functional[23] with the 6-31+G(d,p) basis set. Frequencies, zero-point vibrational energy (ZPVE) corrections and enthalpies were calculated at the same level of theory.

Results

Crystal Structures. The crystal structure of *cc*-DPB has been determined by X-ray diffraction.[15] The four-molecule asymmetric unit shown in Figure 2 reveals equal populations of two conformers, one of which has the two phenyls in parallel planes and the other has the two phenyls in almost perpendicular planes. The two conformers have an average phenyl/diene dihedral angle of 40° and are arranged edge-to-face in alternating layers. In contrast to *cc*-DPB,[15] X-ray crystal diffraction measurements reveal a single *cc*-DTB conformer structure whose two phenyl rings lie in roughly parallel planes oriented at 55.8° to the plane of the diene moiety (Figure 3). The crystal packing arrangement also differs significantly with the *o*-tolyl groups of neighboring *cc*-DTB molecules displaying neither π,π-stacking nor edge-to-face interactions (see the Supporting Information for details on the crystal structure of *cc*-DTB). The closest approaches between neighboring molecules are between the para H of the tolyl group of one and one of the tolyl C atoms bearing the diene moiety of the other. The major steric effect of *o*-methyl substitution on the molecular structure of *cc*-DPB is a 16° widening of the aryl/diene dihedral angle.

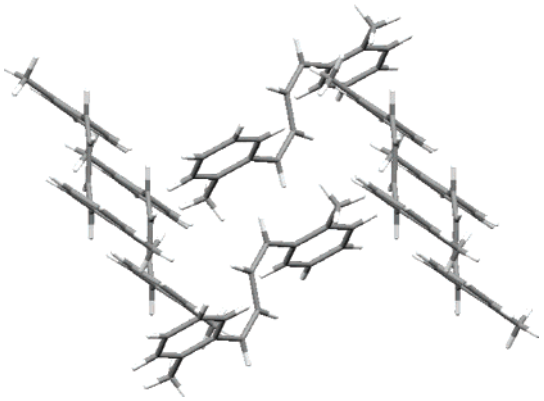

Figure 3. X-ray structure of *cc*-DTB. There are six molecules in the asymmetric unit, four of which are viewed roughly end on.

Photochemical Observations. *cc- and tt-DPB.* The fluorescence spectrum of *cc*-DPB crystals at ambient temperature is a broad structureless band in the 360−600 nm range with λ_{max} = 408 nm. It is independent of excitation wavelength (300−370 nm) and resembles the spectrum obtained at 77 K in isopentane glass.[15] The fluorescence spectra measured in the course of irradiation at 370 nm directly in the sample compartment of the fluorimeter are typical (Figures 4 a−c). ^{1}H NMR analysis of the crystal ($CHCl_3$) at the end of this 8 h irradiation shows the presence of *tt*-DPB as the sole reaction product.

Recrystallization of *tt*-DPB from ethanol gives thin, platelike crystals[2a] that are photochemically inert[24] and are not suitable for structure determination by X-ray diffraction. Crystals, suitable for structure determination by X-ray diffraction, were recently obtained by allowing ethanol to diffuse slowly into a solution of *tt*-DPB in chloroform.[25] Fluorescence spectra of both crystal forms, Figure 5a, are similar and are only subtly structured. A somewhat more structured fluorescence spectrum has been reported from *tt*-DPB crystals obtained on the addition of hexane to a methylene chloride solution of *tt*-DPB.[26] Interestingly, preliminary observations show that in contrast to the platelike *tt*-DPB crystals that are inert, irradiation of the crystals from ethanol/chloroform at 366 nm with a 200 W medium-pressure Hg lamp causes the development of structure in the fluorescence spectra, Figure 5b, concomitant with the appearance of ^{1}H NMR signals in the δ 3.7−4.1, 6.4−6.6, and 7.0−7.2 ranges. Assignment of the area of the signals in the δ 3.7−4.1 region to cyclobutane hydrogens gives an estimate of 19% conversion to photodimer after 3 h of irradiation. No peaks corresponding to DPB photoisomerization products were observed.

The photoisomerization of *cc*-DPB powder was also followed by monitoring changes in fluorescence excitation spectra and powder X-ray diffraction measurements in the course of irradiation at 366 nm using the 200 W Hanovia Hg lamp (Corning glass filters 0-52 and 7-54). The fluorescence excitation spectra are shown in Figure 6. The excitation spectrum of pure *cc*-DPB powder is a broad band with λ_{max} = 370 nm. With photoisomerization to *tt*-DPB, the fluorescence excitation spectrum narrows progressively, gaining in intensity as λ_{max} shifts to 377 nm.

Powder X-ray diffraction measurements establish the crystal-to-crystal nature of the photoisomerization (Figure 7). The diffraction profile of *cc*-DPB (curve a) is very close to that calculated from the X-ray crystallographic diffraction data.[17] The diffraction profile of the crystalline *tt*-DPB photoproduct (curve c) differs significantly from that of ordinary *tt*-DPB crystals (curve d). The ^{1}H NMR spectrum of the irradiated

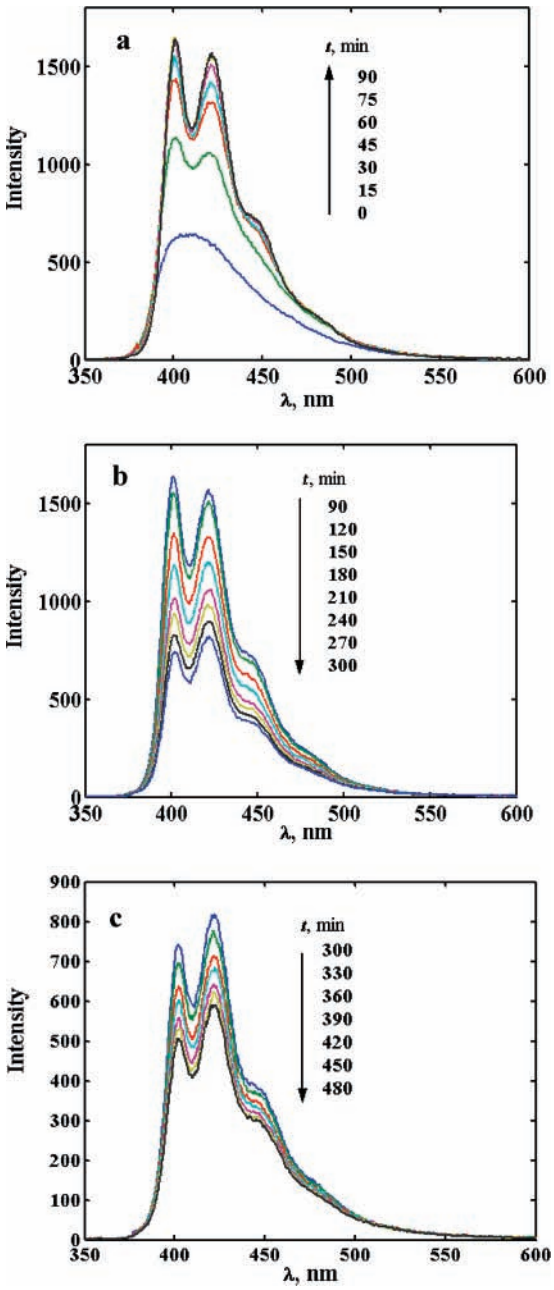

Figure 4. (a−c) Fluorescence spectra obtained over 8 h of irradiation of *cc*-DPB crystals directly in the fluorimeter.

powder at the end of this experiment showed 90% conversion to *tt*-DTB and 10% to dimer.

cc-DTB. Irradiation of solid *cc*-DTB in either crystal or powder form was carried out at ambient temperature as described for *cc*-DPB. Fluorescence spectra for a typical experiment are shown in Figures 8a and 8b. For this experiment, spectra were recorded at the time intervals indicated in the figure as the sample was irradiated in the fluorimeter's sample compartment at 350 nm for 180 min using the fluorimeter's lamp as the light source (reaction is confined by the excitation slit of the fluorimeter to a small horizontal reaction zone) and for an additional 20 h at 366 nm using an external 150 W Xe lamp and monochromator. ^{1}H NMR analysis of the irradiated solid dissolved in $CDCl_3$ showed 8% conversion to *tt*-DTB as the sole reaction product. The final spectrum closely resembles that of a pure *tt*-DTB crystal (Figure 9).

Fluorescence spectra recorded over the course of 6 h of irradiation of *cc*-DTB crystals in the fluorimeter at 315 nm

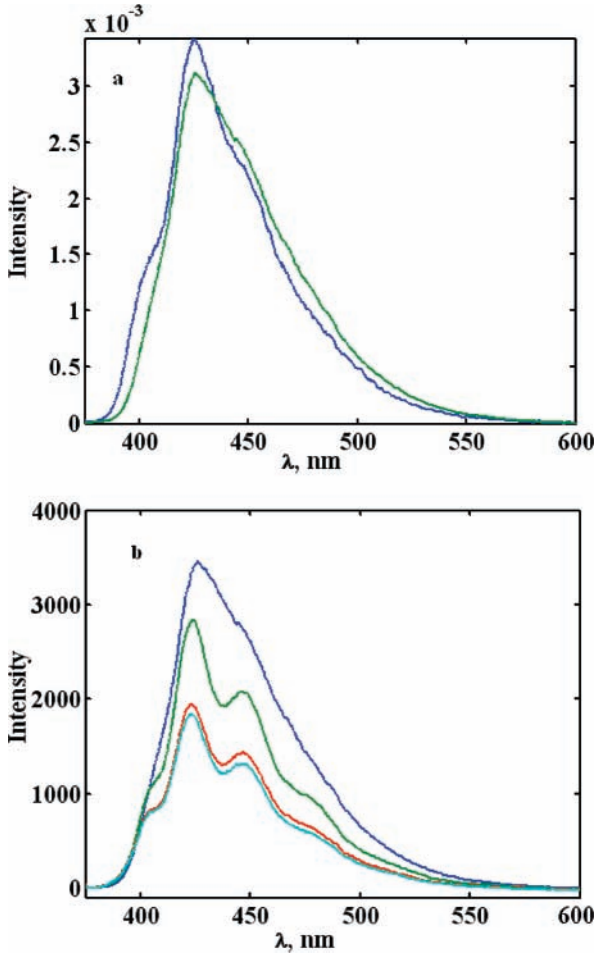

Figure 5. (a) Normalized fluorescence spectra of platelike (blue) and needlelike (green) *tt*-DPB, $\lambda_{exc} = 370$ nm. (b) Fluorescence spectra recorded in the course of 366 nm irradiation (200 W Hanovia lamp) of the crystals obtained from ethanol/$CHCl_3$: 0 h (blue), 1 h (green), 2 h (red), 3 h (cyan), $\lambda_{exc} = 370$ nm.

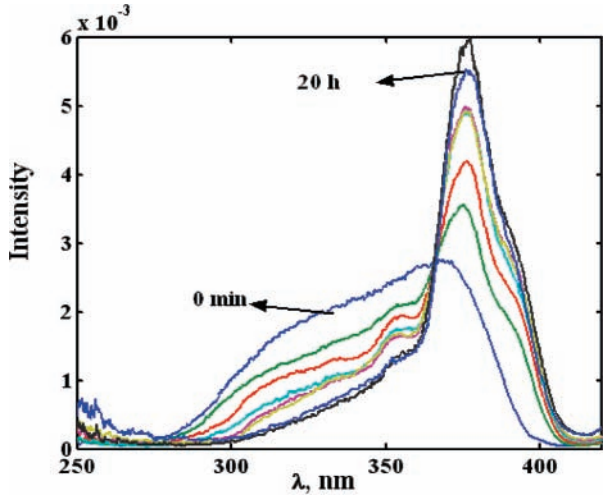

Figure 6. Excitation spectra measured over the course of 20 h of irradiation of *cc*-DPB powder at 366 nm by monitoring emission at 426 nm.

followed by 5.5 h of external irradiation at 313 nm using a 450 W Hanovia medium-pressure Hg lamp are shown in Figure 10. In this experiment, ^{1}H NMR analysis of the irradiated solid dissolved in $CDCl_3$ showed 2% conversion to *tt*-DTB as the sole reaction product. Conversions measured by ^{1}H NMR analysis vary from experiment to experiment, the highest

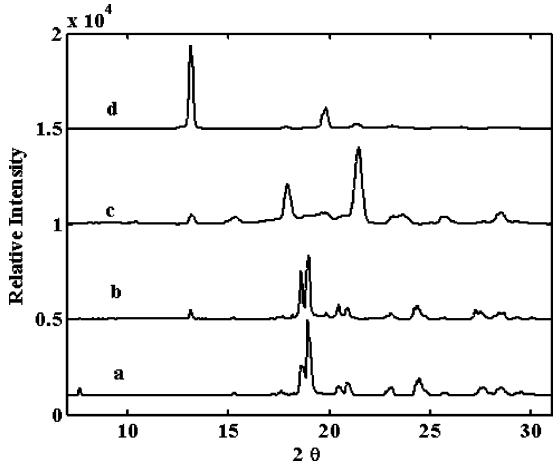

Figure 7. Powder X-ray diffraction profiles of (a) *cc*-DPB, (d) *tt*-DPB, and two irradiated *cc*-DPB samples; conversions to *tt*-DPB by ^{1}H NMR: (b) 16% and (c) 90%.

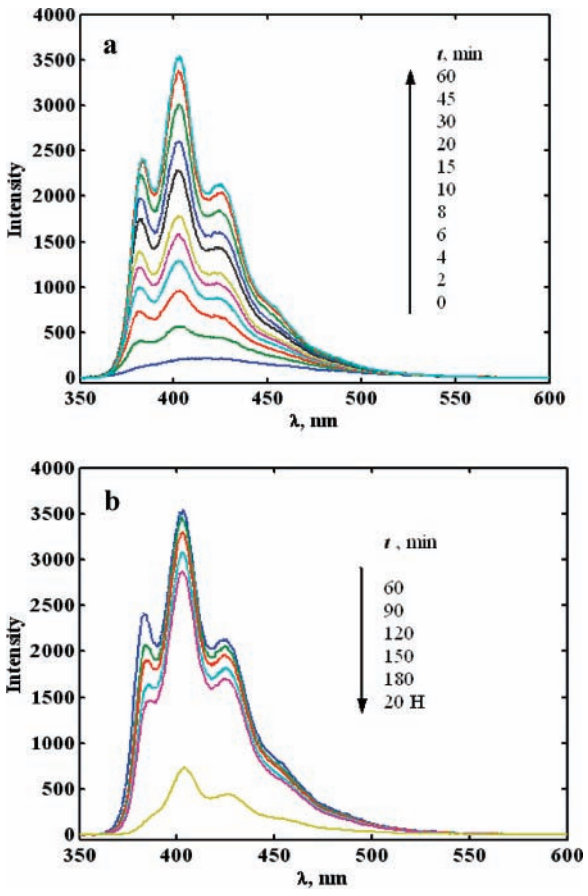

Figure 8. (a) Fluorescence spectra ($\lambda_{exc} = 350$ nm) of solid *cc*-DTB (0 time, blue) and over the course of irradiation ($\lambda_{ir} = 350$ nm for 1 h in the fluorimeter). (b) Irradiation continued for 2 h in the spectrometer at 350 nm and, externally, for an additional 20 h at 366 nm.

achieved being 20% on irradiation of both sides of the glass slides sandwiching the sample (Figure 11). The photoisomerization of *cc*-DTB powder was also evident in changes in the fluorescence excitation spectra. Excitation spectra obtained over the course of 20 h of irradiation of *cc*-DTB at 313 nm (using the 150 W Xe lamp/monochromator combination for the first 8 h and a 450 W Hanovia Hg lamp for the remaining 12 h) are shown in Figure 12. Changes in the shape of the fluorescence spectra were similar to those shown in Figures 8 and 10. The

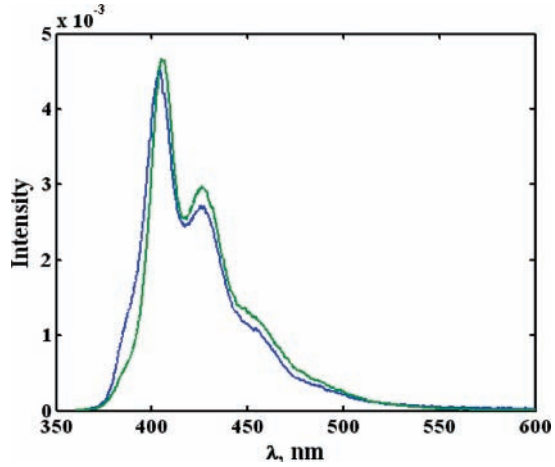

Figure 9. (a) Comparison of the final product emission spectrum from the irradiation of solid *cc*-DTB (blue) with that of pure *tt*-DTB crystal (green), $\lambda_{exc} = 350$ nm.

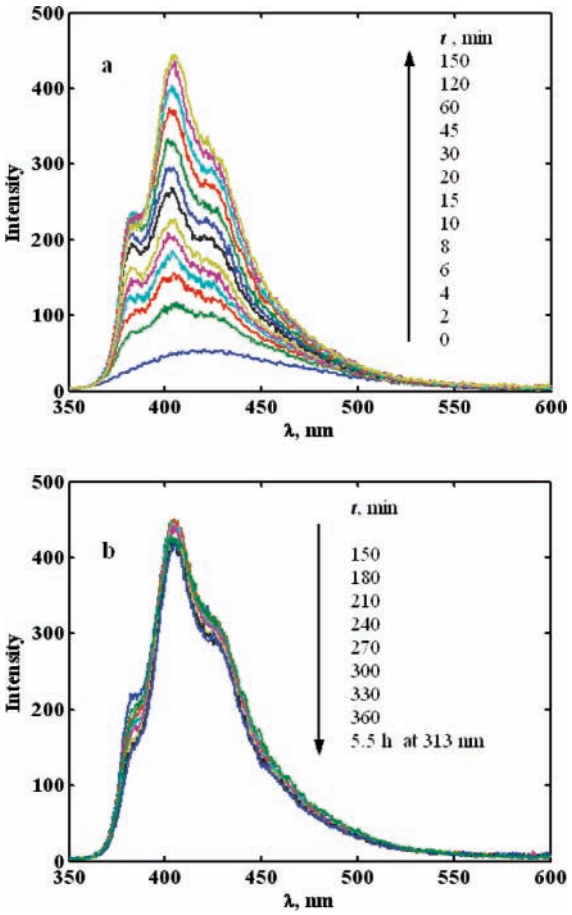

Figure 10. (a) Fluorescence spectra ($\lambda_{exc} = 315$ nm) of solid *cc*-DTB (0 time, blue) and over the course of irradiation ($\lambda_{ir} = 315$ nm for 150 min in the fluorimeter). (b) Irradiation continued for 210 min at 315 nm in the spectrometer and, externally, for an additional 5.5 h at 313 nm.

^{1}H NMR spectrum of the irradiated powder at the end of this experiment showed 7% conversion to *tt*-DTB.

Calculated Structures. Gaussian 98[21] B3LYP calculations with the 6-31G(d,p) basis set predict that in the gas phase the global energy minimum of *cc*-DPB corresponds to the structure with each of the two phenyl moieties rotated in opposite directions 31.5° to the diene plane. The structure with the phenyls in parallel planes rotated 39.6° to the diene plane is predicted to lie 1.5 kcal/mol above it (Figure 13; see ESI in ref 15 for details on the calculated structures of *cc*-, *ct*-, and *tt*-DPB).[15] The latter structure is almost identical to the upper X-ray conformer structure shown in Figure 3.

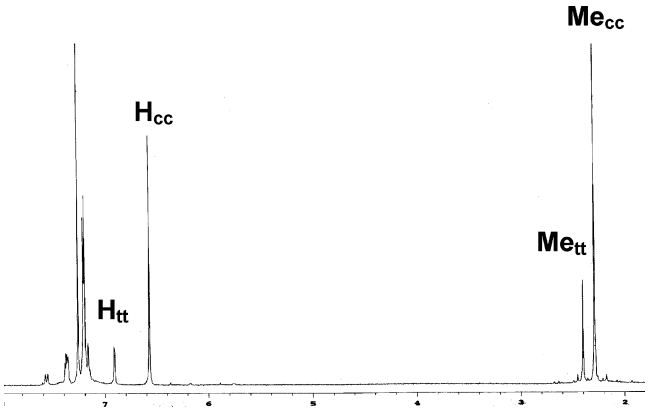

Figure 11. ^{1}H NMR spectrum of solid *cc*-DTB irradiated on both sides for a total exposure period of 20 h. The vinyl and methyl H signals of starting material and product are labeled.

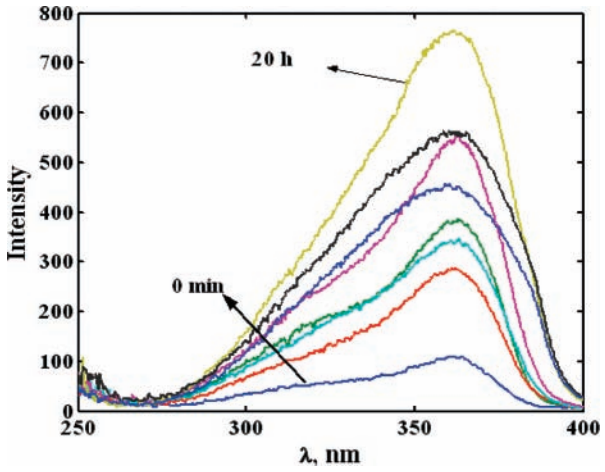

Figure 12. Excitation spectra measured over the course of a 20 h 313 nm irradiation of *tt*-DPB powder by monitoring emission at 420 nm.

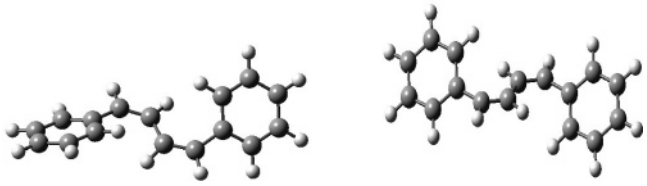

Figure 13. Stationary point geometries on the *cc*-DPB S_0 surface. The structure on the left corresponds to the global energy minimum.

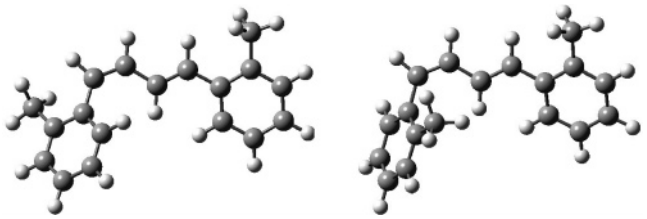

Figure 14. Stationary point geometries on the *ct*-DTB S_0 surface. The structure on the left corresponds to the global energy minimum.

Calculations at the same level of theory were performed only for *ct*-DTB. The structures of the two conformers with respect to rotation of the *o*-tolyl−vinyl bond in the cis portion of the molecule in S_0 are shown in Figure 14. The structure on the left corresponds to the global energy minimum and has dihedral angles between the *o*-tolyl and the diene planes of 42.1° and

SCHEME 3: Solid-State Photoisomerization of *cc*-DPB and *cc*-DTB by the Two-Step BP Mechanism

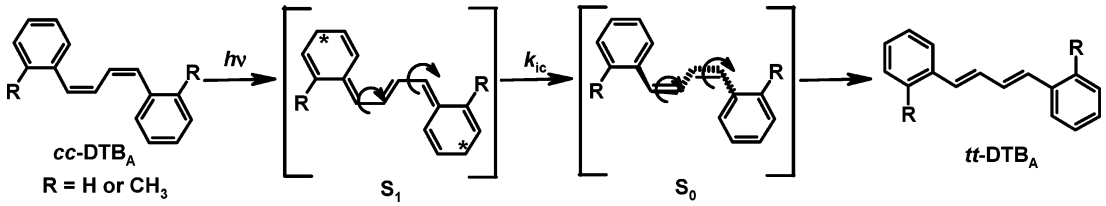

19.7° on the cis and trans sides of the molecule, respectively. The structure on the right is 1.95 kcal/mol higher in energy in the gas phase and has dihedral angles between the *o*-tolyl and the diene planes of 62.0° and 20.8° on the cis and trans sides of the molecule, respectively.

Discussion

Prior to our work,[17] photochemical investigations of solid-state DPB and derivatives were confined to the photodimerization of trans,trans isomers. There are no reports of trans → cis photoisomerization of *tt*-DPB or its derivatives in the solid state. Conventional crystallization of the parent *tt*-DPB gives hexagonal platelike crystals,[2a] which have long been known to be light-stable.[24] It was reasoned that the relative orientation of neighboring molecules was not conducive to photodimer formation despite the close proximity of the central C_2-C_3 bonds, because the terminal C_1-C_2 bonds are far apart. Favorable face-to-face orientation and proximity of the double bonds of neighboring molecules was achieved in derivatives of *tt*-DPB. Such derivatives photodimerize in the solid state, yielding high conversions to specific [2 + 2] photodimers.[24,26−28] In every case the substituent(s) account(s) for product specificity by controlling the relative orientation of *tt*-DPB pairs. The X-ray structure of a new crystalline modification of *tt*-DPB, obtained by crystallization induced upon slow diffusion of ethanol into a chloroform solution of *tt*-DPB, revealed a rather complex packing arrangement containing three distinct *tt*-DPB conformers differing in small deviations from planarity.[25] We were encouraged to carry out a preliminary investigation of the irradiation of such crystals because π,π stacking interactions in some directions brought C═C double bonds of neighboring molecules sufficiently close and in proper orientation to allow photodimerization. ^{1}H NMR analysis of the irradiated crystals obtained from ethanol/$CHCl_3$ reveals the formation of a cyclobutane photodimer, and the progress of the reaction is reflected in the change of the fluorescence spectra shown in Figure 5b.

Cis → trans photoisomerization was considered a rare event in the solid state.[29] However, significant recent activity in this research area suggests a wider scope.[30] We initiated the investigation of the photochemistry of solid *cc*-DPB because the edge-to-face packing of molecules in the crystal[15] appeared to provide significant free volume in the vicinity of the central diene moiety (Figure 1).[17] We reasoned that because edge-to-face phenyl/phenyl interactions tend to anchor the phenyl rings in place, severely restricting their ability to undergo large-amplitude torsional displacement, excitation of at least the conformer with phenyls in parallel planes in *cc*-DPB crystals could promote two-bond isomerization by the BP mechanism. Our expectation was confirmed.[17] ^{1}H NMR and HPLC analyses establish that *tt*-DPB is the only photoisomerization product (see Figure 3 in ref 17), and the powder X-ray diffraction patterns in Figure 7 reveal the crystal-to-crystal nature of the reaction in almost quantitative conversion. Most of the new peaks that emerge in the powder X-ray diffraction pattern on irradiation are present in the diffraction pattern of the platelike *tt*-DPB crystals, but their relative intensities differ markedly, indicating that the photoproduct forms in a different crystalline modification dictated by the arrangement of the *cc*-DPB molecules in the crystal lattice.

As shown in Figure 3, only the conformer with the aryl moieties in parallel planes exists in the *cc*-DTB crystal. *o*-Methyl substitution widens the torsional angle between the aryl and the diene planes from 40° in *cc*-DPB to 56° in *cc*-DTB. The packing patterns of the parent *cc*-DPB and the dimethyl derivative *cc*-DTB differ significantly. *cc*-DTB shows π,π-stacking interactions that are absent in *cc*-DPB, but edge-to-face orientation of the aryl groups of neighboring molecules is evident in both. It is not surprising therefore that ^{1}H NMR analysis of UV-irradiated *cc*-DTB shows the formation of *tt*-DTB as the only product (Figure 11). The difference is that in this case low conversions have thwarted attempts to follow the photoreaction by powder X-ray diffraction measurements.

The steric effect of the *o*-methyl substituents is also evident in the UV spectrum of *tt*-DTB in solution (Figure 1), which is less structured than the spectrum of *tt*-DPB.[2] This suggests a significant departure from planarity, consistent with the calculated 20° *o*-tolyl/diene torsional angles on the trans side of the two lowest-energy *ct*-DTB conformers (Figure 14). Our UV spectra of the DTB isomers are only slightly shifted relative to those of the DPB isomers.[2] They bring into question an earlier report of the UV spectrum of *tt*-DTB, which claimed that λ_{max} = 274 nm and log ϵ_{max} = 4.42 in ethanol.[31]

Bicycle-Pedal Mechanism. In both *cc*-DPB and *cc*-DTB, the emissions of the pure solid cis,cis isomers are structureless, closely resembling the fluorescence spectra of pure *cc*-DPB[15] and *cc*-DTB[32] in isopentane glass at 77 K. The structureless initial *cc*-DPB and *cc*-DTB fluorescence spectra, and the build up of structure in the course of the irradiation show that the two bond photoisomerizations to *tt*-DPB and *tt*-DTB, respectively, are not adiabatic. Because *tt*-DPB and *tt*-DTB products form in their ground state, the BP mechanism must include S_1 and S_0 stages: a first stage in S_1 that brings the molecule to a conical intersection[33] where $S_1 \rightarrow S_0$ internal conversion (k_{ic}) occurs and a second stage in S_0 where the BP motion is completed (Scheme 3). Weiss and Warshel first proposed the idea that torsional momentum in the excited state may carry through the internal conversion into the ground state without hesitation at some twisted excited-state intermediate.[34] Local heating and softening of the surrounding lattice as the initially formed vibrationally hot ground state relaxes to lower vibrational levels should further facilitate product formation.

In view of significant differences in (1) conformer homogeneity, (2) crystal packing arrangements, and (3) extent of conversion to the trans,trans isomers, the observed time evolutions of the fluorescence spectra on irradiation of solid *cc*-DPB and *cc*-DTB are remarkably similar. In both cases, irradiation leads to a gain in fluorescence intensity and development of vibronic structure. Starting from *cc*-DPB (λ_{max} = 408 nm), the spectrum gains in intensity as it develops structure, with λ_{max}

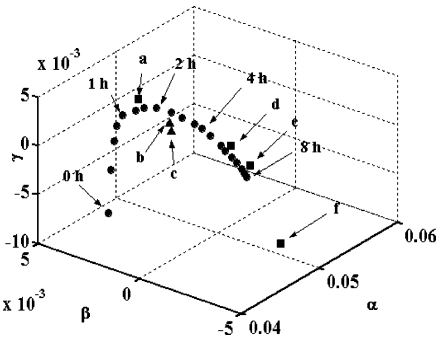

Figure 15. Three-dimensional (α_i, β_i, γ_i) combination coefficient plot for the four-component matrix consisting of the spectral set in Figure 4 (circles, points corresponding to 0, 1, 2, 4, and 8 h irradiation times are indicated) and typical spectra of crystalline (triangles) and powdered (squares) samples irradiated with Hanovia Hg lamps. Conversions to *tt*-DPB determined by ^{1}H NMR spectroscopy are (a) 15%, (b) 13%, (c) 27%, (d) 20%, (e) 48%, and (f) 64%.[17]

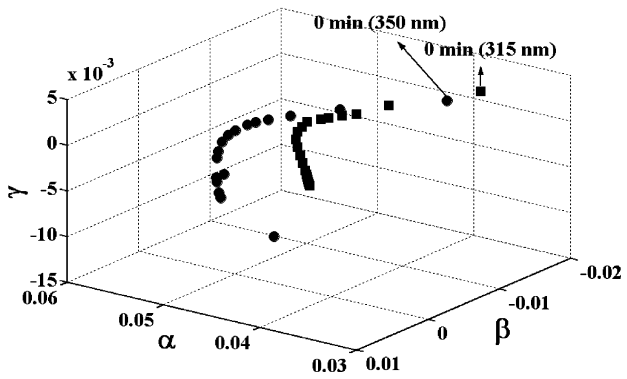

Figure 16. Combination coefficients for the spectral matrix composed of the spectra in Figures 8 (circles) and 10 (squares).

at 402 nm and vibronic bands at 422 and 450 (shoulder) nm (Figure 4). Prolonged irradiation leads to attenuation in overall intensity, broadening at long λ, and a shift of the λ_{max} from 402 to 422 nm. Peak-to-valley intensity ratios show a small dependence on excitation wavelength. Development of structured fluorescence is consistent with the formation of relatively planar *tt*-DPB product. However, it differs significantly from the fluorescence of the two modifications of pure *tt*-DPB crystals that we examined (Figure 5a). Initially, the very subtly structured emissions of both platelike and needlelike *tt*-DPB crystals (obtained from ethanol/$CHCl_3$) are similar with $\lambda_{max} = 426$ nm. Structured fluorescence emerges over the course of photodimerization of the needlelike crystals. With irradiation, the intensity decreases, and well-defined vibronic bands emerge at 420 (λ_{max}) and 447 nm along with shoulders at 405 and 480 nm (Figure 5b). We conclude that the fluorescence spectrum of *tt*-DPB in the solid state is highly sensitive to its microenvironment. However, the relationship of fluorescence shape to microenvironment is less than straightforward as demonstrated by the similarity of the fluorescence spectra of two significantly different crystal packing arrangements of *tt*-DPB in Figure 5a.

Analogous changes are observed on irradiation of *cc*-DTB at 350 nm. Starting from the weak structureless *cc*-DTB spectrum (λ_{max} at 420 nm), there is a rapid gain in intensity as structured emission develops during the first hour with λ_{max} at 404 nm, resolved vibronic bands at 381 and 424 nm, and a shoulder at ~450 nm (Figure 8). Irradiation in the spectrometer for another 2 h leads to a drop in fluorescence intensity, with the loss being more pronounced at the 381 nm peak (Figure 9b). This trend continues on external irradiation until the spectrum becomes almost identical to that of a *tt*-DTB crystal and insensitive to further irradiation (emission spectra obtained after 16, 19, and 20 h irradiations are indistinguishable; Figures 8 and 9). Somewhat less structured spectra are obtained by irradiating the solid sample at 315 nm (Figure 10). The emission intensity maximum shifts from 420 to 405 nm, and shoulders develop at 385 and 430 nm. Prolonged irradiation leads to a decrease in the relative intensity at 385 nm. The spectrum obtained at the end of the initial 6 h irradiation period is independent of λ_{exc} in the 300−360 nm range.

PCA Treatment of Fluorescence Spectral Matrices. Conversions determined by ^{1}H NMR or HPLC for solid samples (crystals or powder) irradiated in the fluorimeter were generally small (2−8%) because the excitation slit of the fluorimeter confines light exposure of the sample to a small horizontal reaction zone. Complete conversions of *cc*-DPB to the trans,-trans isomer (along with small dimer contributions) on external uniform irradiation of the entire sample were achieved, but the same procedure failed to increase conversions in the case of *cc*-DTB. For *cc*-DPB, the relationship of the shape of the fluorescence spectrum to actual conversion was determined by simultaneous PCA treatment of the spectra in Figure 4 and fluorescence spectra of crystals (or powder) that were more uniformly exposed to 366 nm light from a 200 W medium-pressure Hanovia Hg lamp for different time periods and for which conversions to *tt*-DPB were independently measured by ^{1}H NMR. Minor conversions to photodimers (~10% of total conversion) that do not contribute to the fluorescence spectra are also evident in the ^{1}H NMR spectra. The PCA treatment reveals a four-component system. The experimental spectra, *S*, *i*, are reproduced (with random noise suppressed) as linear combinations of the four principal eigenvectors ($\mathbf{V}_\alpha$, $\mathbf{V}_\beta$, $\mathbf{V}_\gamma$, and $\mathbf{V}_\delta$)

$$S_i = \alpha_i \mathbf{V}_\alpha + \beta_i \mathbf{V}_\beta + \gamma_i \mathbf{V}_\gamma + \delta_i \mathbf{V}_\delta \qquad (1)$$

A plot of the combination coefficients (α_i, β_i, γ_i) of the three major eigenvectors is shown in Figure 15.

The combination coefficients of fluorescence spectra from samples for which ^{1}H NMR conversions are available fall on the same plane, close to the parabola, and provide a means, albeit not quantitative, of relating the shape of the fluorescence spectrum to the percentage conversion to *tt*-DPB. The photoisomerization is more rapid initially and then slows down, eventually leading to complete *cc*-DPB depletion. In Figure 4, spectra were measured every 15 min for the first 90 min, the fast reaction stage, and then every 30 min for the 90−480 min irradiation period corresponding to slower reaction stages. We had initially speculated that the reaction proceeds in stages[35] in part due to different BP photoreactivity of the two *cc*-DPB conformers.[17] However, the similar time evolutions of the fluorescence spectra obtained on the irradiation of solid *cc*-DTB tend to make that argument less secure. A highly conformer-specific crystal-to-crystal photoreaction in a two-layer crystal was reported recently.[36]

PCA treatments[20] of the matrices consisting of the spectra in Figures 8 and 10 reveal four- and three-component systems, respectively. Including the spectra in Figures 8 and 10 in a global PCA treatment again gives a four-component system, showing that no additional components are introduced on excitation at 313/315 nm. The combination coefficients (α_i, β_i, γ_i) of the three major eigenvectors for the combined matrix are plotted in Figure 16. Spectral points move on two concentric parabolic trajectories on the same α_i, β_i, γ_I plane. Plots of the combination coefficients in α_i, β_i, δ_i space are also consistent with smooth spectral progressions.

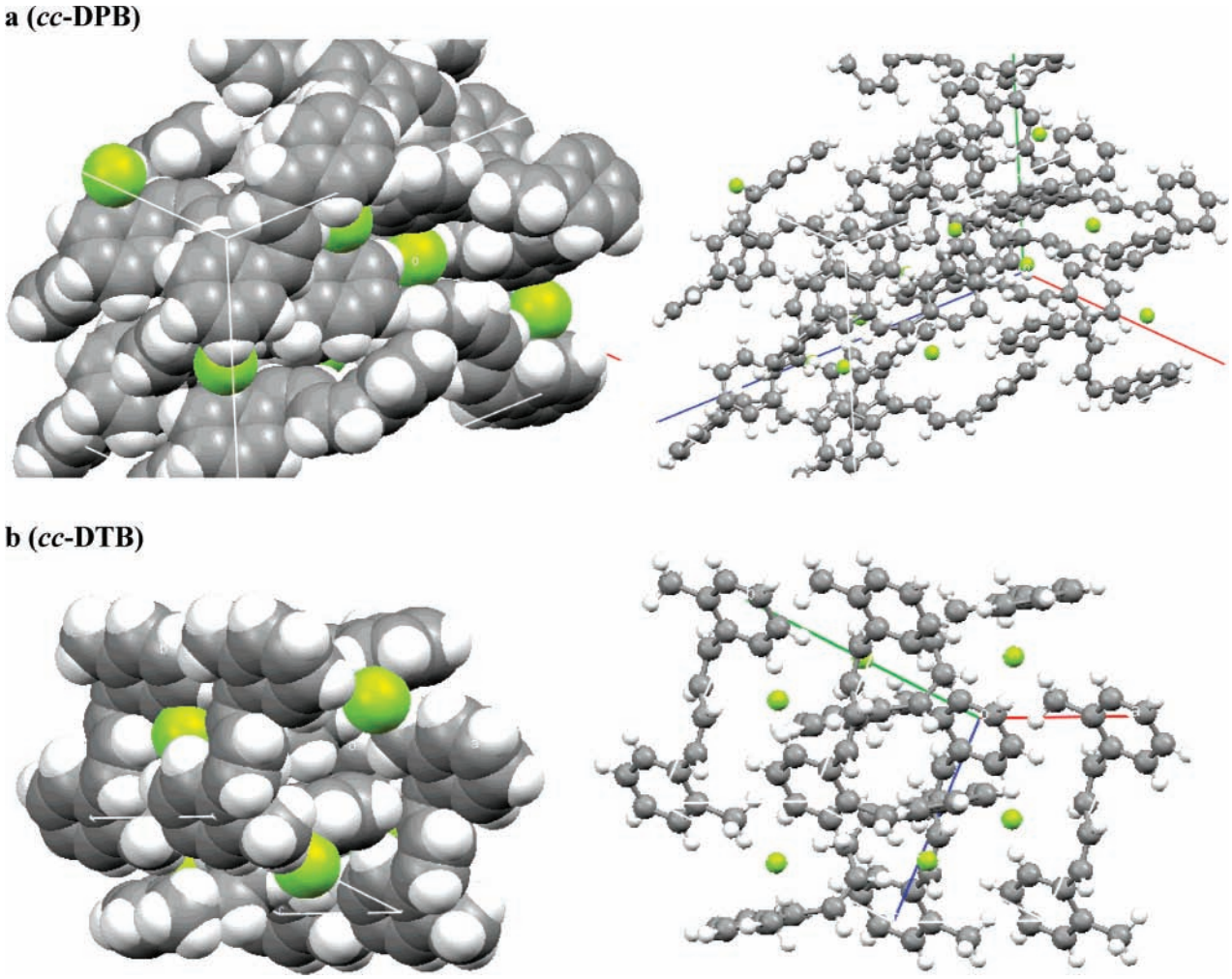

Figure 17. PLATON-generated spherical cavity plots (green) with (a) probe radii of 1.01−1.05 Å for *cc*-DPB and (b) a probe radius of 0.75 Å for *cc*-DTB. Space-filling and ball-and-stick figures of the same projection are shown on the left and on the right, respectively.

The red shifts in the fluorescence excitation spectra over the course of product formation (Figures 6 and 12) indicate that trans,trans product sites can potentially function as low-energy traps. Energy migration to product sites might lead to inhibition of the photoreaction by the product, providing an explanation for fast and slow reaction stages in *cc*-DPB and low product yields in *cc*-DTB. However, the deviations of points from the parabola in Figure 15 and the concentric parabolas in Figure 16, depending on the excitation wavelength, show that different *tt*-DPB and *tt*-DTB product sites in the *cis,cis* crystal lattices can be excited selectively. Furthermore, the fact that fluorescence is observed simultaneously from as many as three different product sites for both DPB and DTB (the starting cis,cis isomers are the fourth components) indicates that, at least initially, singlet excitation energy does not efficiently migrate to the lowest-energy trap. These results suggest that the fluorescence spectra of *tt*-DPB and *tt*-DTB are controlled by their crystalline microenvironment. Although we cannot rule out energy transfer as the reason for the low conversions in the *cc*-DTB crystals, the buildup of lattice strain over the course of *tt*-DTB formation may also contribute to reaction inhibition. The similarity of the final fluorescence spectrum from the irradiation of *cc*-DTB to that of the pure *tt*-DTB crystal is consistent with the finding that *tt*-DTB is the photoproduct. However, that does not require neighboring *tt*-DTB molecules to be similarly arranged in the two crystals. The differences between the fluorescence spectra in Figure 9 and those in the fluorescence spectra of the two crystalline modifications of *tt*-DPB in Figure 5a are very similar, despite probable differences in molecular packing arrangements in the latter.[25]

Correlation of Photoreactivity with Cavities in the Crystal Lattice. Moorthy, Weiss, and co-workers recently described a method for evaluating the ability of individual molecules in a crystal lattice to undergo the atomic motions required for cis → trans isomerization based on the size and location of cavity volumes in the crystal.[30c] Using the PLATON program,[37] they generated "cavity plots" by finding locations within the unit cell that could accommodate spherical "probe species" with specified radius *r*. The percentage void volume, taken as the sum of the volumes of such spheres relative to the volume of the unit cell, increased as the selected *r* value was decreased in 0.05 Å steps from 1.1 to 0.5 Å. Smaller *r* values identify void spaces that were considered too small to be useful in understanding molecular dynamics. Because real cavities in the crystal lattice are not spherical, this method locates hole components that are expected to be contained in much larger spaces where groups of covalently attached atoms are not packed with sufficient efficiency to leave only interstitial volumes[38] between them.[30c] Spherical voids with $r \geq 0.80$ Å were considered sufficiently large to permit cis → trans photoisomerization, provided that they were located close to molecular moieties undergoing large-amplitude displacements.

Using that method we were able to show that the crystal lattice of *cc*-DPB readily accommodates voids of $r = 1.05$ Å

(Figure 17a). Many more cavities are located for $r = 1.00$ Å. These large spherical cavities are located closer to the phenyl rings than to the diene moieties. In contrast, the maximum size of spherical voids in the crystal lattice of *cc*-DTB were found for $r = 0.75$ Å (Figure 17b). Although smaller, they are conveniently located in the vicinity of the diene moieties and may account for their ability to undergo the space-conserving BP process. Significantly less compact packing in *cc*-DPB may explain the much larger conversion to the trans,trans photoproduct in this case.

Conclusion

Intermolecular interactions, including edge-to-face attractions of the phenyl and *o*-tolyl groups in the crystal lattices of *cc*-DPB and *cc*-DTB, respectively, restrict significant displacement of these moieties, confining most of the photoisomerization motion to the central diene unit and minimizing free volume requirements.[30] Significantly larger empty cavities in *cc*-DPB than in *cc*-DTB may account for the much higher conversions to the trans,trans isomer in *cc*-DPB. It is significant that, as in the case of the muconates,[39] the diene moiety in S_1 chooses the BP photoisomerization pathway (Scheme 3). This is consistent with HOMO/LUMO considerations, which predict reversal of single/double bond character on excitation to S_1. Accordingly, S_1 is depicted as a quinoid structure in Scheme 3. Reversal of single/double bond character is at the heart of Havinga's nonequilibration of excited rotamers (NEER) principle, accounting for the well-established conversion of freely interconverting conformers in S_0 of conjugated systems into non-interconverting isomers in S_1.[40] Relevant examples include the diene moiety in *tt*-DPB[41] and the naphthyl moiety in *trans*-1-(2-naphthyl)-2-phenylethene.[20a]

In addition to DPB, its derivatives,[15,17,18] and the muconates[39] in solid or glassy media, other reports of two-bond photoisomerizations indicate that the BP process in polyenes may not be a rare event. The interconversion of *cis,trans,trans*-1,6-diphenyl-1,3,5-hexatriene (*ctt*-DPH) and *tct*-DPH isomers are likely BP photoisomerization examples in solution.[42] The BP process probably also accounts for the two-bond photoisomerizations of *ctc*-DPH derivatives to the *ttt*-DPH isomers in the solid state.[43]

Acknowledgment. This research was supported by the National Science Foundation (Grant No. CHE-0314784). We thank Dr. Mariappan Manoharan for the density functional theory calculations and Dr. Donny Magana for assistance with the powder X-ray diffraction measurements.

Supporting Information Available: Cartesian coordinates, drawings, and total energies of optimized structures (minima on S_0) using B3LYP/6-31+G(d,p) for *cis,trans*-1,4-di-*o*-tolyl-1,3-butadiene. Crystallographic information files for *cc*-DTB X-ray structures, and tables of X-ray data for *cis,cis*-1,4-di-*o*-tolyl-1,3-butadiene consisting of crystallographic parameters, positional parameters, bond distances, bond angles, and torsional angles. This information is available free of charge via the Internet at http://pubs.acs.org.

References and Notes

(1) For reviews, see (a) Saltiel, J.; Sun, Y.-P. Cis−Trans Isomerization of C,C Double Bonds. In *Photochromism, Molecules and Systems*; Dürr, H., Bouas-Laurent, H., Eds.; Elsevier: Amsterdam, 1990; pp 64−164. (b) Saltiel, J.; Charlton, J. L. Cis−Trans Isomerization of Olefins. In *Rearrangements in Ground and Excited States*; de Mayo, P., Ed.; Academic Press: New York, 1980; Vol. III, pp 25−89.

(2) (a) Sandoval, A.; Zechmeister, L. *J. Am. Chem. Soc.* **1947**, *69*, 553−557. (b) Pinckard, J. H.; Wille, B.; Zechmeister, L. *J. Am. Chem. Soc.* **1948**, *70*, 1938−1944.

(3) Eastman, L. R., Jr.; Zarnegar, B. M.; Butler, J. M.; Whitten, D. G. *J. Am. Chem. Soc.* **1974**, *96*, 2281−2283.

(4) Yee, W. A.; Hug, S. J.; Kliger, D. S. *J. Am. Chem. Soc.* **1988**, *110*, 2164−2169.

(5) (a) Saltiel, J. *J. Am. Chem. Soc.* **1967**, *89*, 1036−1037. (b) Saltiel, J. *J. Am. Chem. Soc.* **1968**, *90*, 6394−6400.

(6) Saltiel, J.; Metts, L.; Wrighton, M. *J. Am. Chem. Soc.* **1970**, *92*, 3227−3229.

(7) (a) Saltiel, J.; Sun, Y.-P. *J. Phys. Chem.* **1989**, *93*, 6246−6250. (b) Sun, Y.-P.; Saltiel, J. *J. Phys. Chem.* **1989**, *93*, 8310−8316. (c) Saltiel, J.; Waller, A. S.; Sears, D. F., Jr. *J. Am. Chem. Soc.* **1993**, *115*, 2453−2465. (d) Saltiel, J.; Waller, A. S.; Sears, D. F., Jr.; Garrett, C. Z. *J. Phys. Chem.* **1993**, *97*, 2516−2522.

(8) (a) Gegiou, D.; Muszkat, K. A.; Fischer, E. *J. Am. Chem. Soc.* **1968**, *90*, 12−18. (b) Sharafi, S.; Muszkat, K. A. *J. Am. Chem. Soc.* **1971**, *93*, 4119−4125. (c) Castel, N.; Fischer, E. *J. Mol. Struct.* **1985**, *127*, 159−166.

(9) Alfimov, M. V.; Razumov, V. F.; Rachinski, A. G.; Listvan, V. N.; Scheck, Yu. B. *Chem. Phys. Lett.* **1983**, *101*, 593−597.

(10) Warshel, A. *Nature* **1976**, *260*, 679.

(11) (a) Liu, R. S. H.; Asato, A. E. *Proc. Natl. Acad. Sci. U.S.A.* **1985**, *82*, 259−263. (b) Liu, R. S. H.; Mead, D.; Asato, A. E. *J. Am. Chem. Soc.* **1985**, *107*, 6609−6614.

(12) Müller, A. M.; Lochbrunner, S.; Schmid, W. E.; Fuss, E. *Angew. Chem., Int. Ed. Engl.* **1998**, *37*, 505−507.

(13) (a) Liu, R. S. H.; Hammond, G. S. *Proc. Natl. Acad. Sci. U.S.A.* **2000**, *97*, 11153−11158. (b) Liu, R. S. H. *Acc. Chem. Res.* **2001**, *34*, 555−562. (c) Liu, R. S. H.; Hammond, G. S. *Chem.—Eur.* **2001**, *7*, 4537−4544. (d) Liu, R. S. H. *Pure Appl. Chem.* **2002**, *74*, 1391−1396. (e) Liu, R. S. H.; Hammond, G. S. *Photochem. Photobiol. Sci.* **2003**, *2*, 835−844. (f) Liu, R. S. H.; Hammond, G. S. In *Handbook of Organic Photochemistry and Photobiology*, 2nd ed.; Horspool, W. M., Lenci, F., Eds.; CRC Press: London 2004; pp 26/1−26/11. (g) Krishnamoorthy, G.; Schieffer, S.; Pescatore, J.; Ulsh, R.; Liu, R. S. H.; Liu, J. *Photochem. Photobiol. Sci.* **2004**, *3*, 1047−1051. (e) Liu, R. S. H.; Hammond, G. S. *Acc. Chem. Res.* **2005**, *38*, 396−403.

(14) Yang, L.; Liu, R. S. H.; Boarman, K. J.: Wendt, N. L.; Liu, J. *J. Am. Chem. Soc.* **2005**, *127*, 2404−2405.

(15) Saltiel, J.; Krishna, T. S. R.; Turek, A. M.; Clark, R. J. *J. Chem. Soc., Chem. Commun.* **2006**, 1506−1508.

(16) For organic glass viscosities, see: (a) Greenspan, H.; Fischer, E. *J. Phys. Chem.* **1965**, *69*, 2466−2469. (b) von Salis, G. A.; Labhart, H. *J. Phys. Chem.* **1968**, *72*, 752−754. (c) Ling, A. C.; Willard, J. E. *J. Phys. Chem.* **1968**, *72*, 1918−1923.

(17) Saltiel, J.; Krishna, T. S. R.; Clark, R. J. *J. Phys. Chem. A* **2006**, *110*, 1694−1697.

(18) Liu, R. S. H.; Yang, L. Y.; Liu, J. *Photochem. Photobiol.* **2007**, *83*, 2−10.

(19) (a) Ciana, D. L.; Haim, A. J. *Heterocycl. Chem.* **1984**, *21*, 607−608. (b) Eglinton, G.; Jones, E.R. H.; Shaw, B. L.; Whiting, M. C. *J. Chem. Soc.* **1954**, 1860−1865 .

(20) (a) Saltiel, J.; Sears, D. F., Jr.; Choi, J.-O.; Sun, Y.-P.; Eaker, D. W. *J. Phys. Chem.* **1994**, *98*, 35−46. (b) Saltiel, J.; Krishna, T. S. R.; Turek, A. M. *J. Am. Chem. Soc.* **2005**, *127*, 6938−6939.

(21) Frisch, M. J.; Trucks, G. W.; Schlegel, H. B.; Scuseria, G. E.; Robb, M. A.; Cheeseman, J. R.; Zakrzewski, V. G.; Montgomery, J. A.; Stratmann, R. E.; Burant, J. C.; Dapprich, S.; Millam, J. M.; Daniels, A. D.; Kudin, K. N.; Strain, M. C.; Farkas, O.; Tomasi, J.; Barone, V.; Cossi, M.; Cammi, R.; Mennucci, B.; Pomelli, C.; Adamo, C.; Clifford, S.; Ochterski, J.; Petersson, G. A.; Ayala, P. Y.; Cui, Q.; Morokuma, K.; Malick, D. K.; Rabuck, A. D.; Raghavachari, K.; Foresman, J. B.; Cioslowski, J.; Ortiz, J. V.; Baboul, A. G.; Stefanov, B. B.; Liu, G.; Liashenko, A.; Piskorz, P.; Komaromi, I.; Gomperts, R.; Martin, R. L.; Fox, D. J.; Keith, T.; Al-Laham, M. A.; Peng, C. Y.; Nanayakkara, A.; Gonzalez, C.; Challacombe, M.; Gill, P. M. W; Johnson, B.; Chen, W.; Wong, M. W.; Andres, J. L.; Gonzalez, C.; Head-Gordon, M.; Replogle, E. S.; Pople, J. A. *Gaussian 98*, revision A.7, Gaussian, Inc., Pittsburgh PA, 1998.

(22) (a) Schlegel, H. B. *J. Comput. Chem.* **1982**, *3*, 214−218. (b) Schlegel, H. B. *Adv. Chem. Phys.* **1987**, *67*, 249−286. (c) Schlegel, H. B. In *Modern Electronic Structure Theory*; Yarkony, D. R., Ed.; World Scientific: Singapore, 1995; p 459.

(23) (a) Becke, A. D. *Phys. Rev. A* **1988**, *38*, 3098−3100. (b) Lee, C.; Yang, W.; Parr, R. G. *Phys. Rev. B* **1988**, *37*, 785−789. (c) Becke, A. D. *J. Chem. Phys.* **1993**, *98*, 5648−5652. (d) Stevens, P. J.; Devlin, F. J.; Chabalowski, C. F.; Frisch, M. J. *J. Phys. Chem.* **1994**, *98*, 11623−11627.

(24) (a) Cohen, M. D.; Green, B. S.; Ludmer, E.; Schmidt, G. M. J. *Chem. Phys. Lett.* **1970**, *7*, 486. (b) Cohen, M. D.; Elgavi, A.; Green, B. S.; Ludmer, E.; Schmidt, G. M. J. *J. Am. Chem. Soc.* **1972**, *94*, 6776−6779.

(25) Glaser, R.; Dendi, L. R.; Knotts, N.; Barnes, C. *Cryst. Growth Des.* **2003**, *3*, 291−300.
(26) Singh, A. K.; Krishna, T. S. R. *J. Phys. Chem. A* **1997**, *101*, 3066−3069.
(27) Warshel, A.; Shakked, Z. *J. Am. Chem. Soc.* **1975**, *97*, 5679−5684.
(28) (a) Liu, J.; Boarman, K. J. *Chem. Commun.* **2005**, 340−314. (b) Liu, J.; Wendt, N. L.; Boarman, K. J. *Org. Lett.* **2005**, *7*, 1007−1010. (c) Liu, J.; Boarman, K. J.; Wendt, N. L.; Cardenas, L. M. *Tetrahedron Lett.* **2005**, *46*, 4953−4956.
(29) For one bond photoisomerization, see: (a) Bregman, K.; Osaki, K.; Schmidt, G. M. J.; Sonntag, F. I. *J. Chem. Soc.* **1964**, 2031−2030. (b) Alfimov, M. V.; Razumov, V. F. *Mol. Cryst. Liq. Cryst.* **1978**, *49*, 95−97. (c) Aldoshin, S. M.; Alfimov, M. V.; Atovmyan, L. O.; Kaminsky, V. F.; Razumov, V. F.; Rachinsky, A. G. *Mol. Cryst. Liq. Cryst.* **1984**, *108*, 1−17. (d) Kaupp, G. *Photochem. Photobiol.* **2002**, *76*, 590−595 and references therein.
(30) (a) Tanaka, K.; Hiratsuka, T.; Ohba, S.; Naimi-Jamal, M. R.; Kaupp, G. *J. Phys. Org. Chem.* **2003**, *16*, 905. (b) Natarajan, A.; Mague, J. T.; Venkatesan, K.; Arai, T.; Ramamurthy, V. *J. Org. Chem.* **2006**, *71*, 1055. (c) Moorthy, J. N.; Venkatakrishnan, P.; Savitha, G. Weiss, R. G. *Photochem. Photobiol. Sci.* **2006**, *5*, 903−913 and references therein.
(31) Hirshberg, Y.; Bergmann, E.; Bergmann, F. *J. Am. Chem. Soc.* **1950**, *72*, 5120−5123.
(32) Saltiel, J.; Bremer, M,; Krishna, T. R. S. *Angew. Chem. Int. Ed. Engl.*, in press.
(33) (a) Olivucci, M.; Bernardi, F.; Celani, P.; Ragazos, I. N.; Robb, M. A. *J. Am. Chem. Soc.* **1994**, *116*, 1077−1085. (b) Celani, P.; Garavelli, M.; Ottani, S.; Bernardi, F.; Robb, M. A.; Olivucci, M. *J. Am. Chem. Soc.* **1995**, *117*, 11584−11585. (c) Garavelli, M.; Celani, P.; Bernardi, F.; Robb, M. A.; Olivucci, M. *J. Am. Chem. Soc.* **1997**, *119*, 11487−11494. (d) Garavelli, M.; Smith, B. R.; Bearpark, M. J.; Bernardi, F.; Olivucci, M.; Robb, M. A. *J. Am. Chem. Soc.* **2000**, *122*, 5568−5581.
(34) Weiss, R. M.; Warshel, A. *J. Am. Chem. Soc.* **1979**, *101*, 6131−6133.
(35) (a) Zimmerman, H. E.; Nesterov, E. E. *Org. Lett.* **2000**, *2*, 1169−1171. (b) Zimmerman, H. E.; Nesterov, E. E. *Acc. Chem. Res.* **2002**, *35*, 77−85. (c) Zimmerman, H. E.; Nesterov, E. E. *J. Am. Chem. Soc.* **2002**, *124*, 2818−2830.
(36) Kobatake, S.; Matsumoto, Y.; Irie, M. *Angew. Chem., Int. Ed.* **2005**, *44*, 2148−2151.
(37) Spek, A. L. *PLATON, A Multipurpose Crystallographic Tool*; Utrecht University: Utrecht, The Netherlands, 2005.
(38) (a) Vrentas, J. S.; Duda, J. L. *J. Polym. Sci., Polym. Phys. Ed.* **1977**, *15*, 403−416. (b) Vrentas, J. S.; Duda, J. L. *J. Polym. Sci., Polym. Phys. Ed.* **1977**, *15*, 417−425. (c) Duda, J. L.; Zielinski, J. M. In *Diffusion in Polymers*; Neogi, P., Ed.; Marcel Dekker: New York, 1996; Chapter 3.
(39) (a) Odani, T.; Matsumoto, A.; Sada, K.; Miyata, M. *Chem. Commun.* **2001**, 2004−2005 and references therein. (b) Matsumoto, A. *Top. Curr. Chem.* **2005**, *254*, 263−305.
(40) Jacobs, H. J. C.; Havinga, E. *Adv. Photochem.* **1979**, *11*, 305−373.
(41) (a) Sun, Y.-P.; Bunker, C. E.; Wickremesinghe, P. L.; Rollins, H. W.; Lawson, G. E. *J. Phys. Chem.* **1995**, *99*, 3423. (b) Bunker, C. E.; Lytle, C. A.; Rollins, H. W.; Sun, Y.-P. *J. Phys. Chem. A* **1997**, *101*, 3214.
(42) (a) Saltiel, J.; Ko, D.-H.; Fleming, S. A. *J. Am. Chem. Soc.* **1994**, *116*, 4099−4100. (b) Saltiel, J.; Wang, S.; Watkins, L. P.; Ko, D.-H. *J. Phys. Chem. A* **2000**, *104*, 11443−11450.
(43) Sonoda, Y.; Kawanishi, Y.; Tsuzuki, S.; Goto, M. *J. Org. Chem.* **2005**, *70*, 9755−9763.